PAPER

Wideband ‘black silicon’ for mid-infrared applications

IOP Publishing Journal of Optics
J. Opt. 19 (2017) 065101 (6pp) https://doi.org/10.1088/2040-8986/aa69d6

Wideband 'black silicon' for mid-infrared applications

K Gorgulu[1], M Yilmaz[2], K Topalli[2,3,4] and A K Okyay[1,2,3,4]

[1] Department of Electrical and Electronics Engineering, Bilkent University, Ankara 06800, Turkey
[2] UNAM-National Nanotechnology Research Center, Bilkent University, Ankara 06800, Turkey
[3] Institute of Materials Science and Nanotechnology, Bilkent University, Ankara 06800, Turkey

E-mail: aokyay@stanfordalumni.org

Received 21 December 2016, revised 18 March 2017
Accepted for publication 29 March 2017
Published 25 April 2017

Abstract

In this paper, we investigate the absorption of mid-infrared light by low resistivity silicon textured via deep reactive ion etching. An analytical description of the wave propagation in black silicon texture is presented, showing agreement with the experiment and the computational analysis. We also study the dependence of absorption spectrum of black silicon structure on the electrical conductivity of silicon substrate. The structures investigated unveil wideband, all-silicon infrared absorbers applicable for infrared imaging and spectroscopy with simple CMOS compatible fabrication suitable for optoelectronic integration.

Keywords: black silicon, absorber, infrared, deep reactive ion etching

(Some figures may appear in colour only in the online journal)

1. Introduction

Electromagnetic (EM) wave absorbers are of great importance for their potential of various applications including chemical and biological sensors, imagers, emission sources, and light harvesting devices. Considerable recent research has focused on increasing the efficiency of energy absorption processes. Highly efficient light absorption in metallic structures has been widely studied in metal–insulator–metal structures, nanoparticles, and arrays of metallic gratings [1–5]. Metamaterial absorbers are also widely explored as promising candidates to enhance EM wave absorption at microwave, terahertz, infrared, and visible frequencies [6–9]. However, confined by resonance nature of the unit structures, these metamaterial absorbers generally absorb light within a narrow wavelength range. Much of the work in this direction focuses on multi-resonance or tapered metamaterial structures to increase bandwidth. Nevertheless, the number of resonators combined within the same unit cell is limited. Moreover, these devices are typically made of metals that are not compatible with CMOS processes (such as Au) and that have degradation problem upon exposure to air and humidity such as Ag.

Alternatively, there are many materials, other than conventional metals, that provide advantages in device performance, integration, and tunability such as semiconductors, transparent conducting oxides, metal nitrides, perovskite oxides, silicides, germanides, and 2D materials [10, 11]. Among these materials, semiconductors have attracted great interest due to their well-established fabrication and integration technology. To date, various plasmonic and metamaterial absorbers have been studied with different semiconductors [12–18]. All-silicon efficient narrowband and broadband absorbers have been studied recently [19–21]. In addition to these absorbers, needle-like black silicon structures emerged as interesting material with broadband absorbance of more than 99% [22, 23]. Several methods are used to obtain black silicon including chemical etching, (deep) reactive ion etching, and laser treatment [24]. So far black silicon structures are presented in the visible and the near-infrared region mostly for photovoltaic and surface enhanced sensing applications [25–27].

In this work, we investigate the absorption properties of black silicon in the mid-infrared region. The starting substrate is a 7.5×10^{19} boron-doped (0.001–0.002 Ωcm) Czochralski-grown silicon wafer with the thickness of $500+/-20$ μm and

[4] Dr Okyay and Dr Topalli were with Bilkent University at the time of the study.

⟨100⟩ orientation. We use scanning electron microscope (SEM) images of the resulting silicon surface and implement the pattern into simulation environment. Furthermore, we use effective medium theory (EMT) to explain interaction of EM wave with black silicon structure. The absorption waveband of black silicon texture is significantly improved compared to that of flat silicon surface. Here, black silicon texture with random pyramidal structures acts like an antireflective coating and absorbs the incoming light by virtue of its high attenuation coefficient (1.7 μm^{-1} around plasma frequency). Classical antireflective designs for broadband operation typically have several thick layers [28]. However, this has the undesirable effect of making the structure bulky. Also, thick layers may cause delaminating of the deposited AR coating [29]. On the other hand, etched mechanical surfaces, like black silicon texture, can provide very broadband antireflective operation without such problems [30]. Broadband operation of black silicon texture can also be fine-tuned by controlling the shape of the individual features and conductivity of the silicon wafer. The mature silicon manufacturing technology could pave the way for CMOS compatible integration for specific applications.

2. Structure and methods

Optical properties of low resistivity semiconductors are dominated by electron plasma of the material, and can be modeled using Drude formalism. According to Drude model, complex permittivity can be calculated as:

$$\varepsilon(\omega) = \varepsilon_\infty\left(1 - \frac{\tau\omega_p^2}{\tau\omega^2 + j\omega}\right), \quad (1)$$

where ε_∞ is the permittivity value for frequency $\omega \gg \omega_p$ and taken as 11.7, τ is the relaxation time, ω_p is the plasma frequency. The formulation of the plasma frequency, ω_p, is given below

$$\omega_p^2 = \frac{Ne^2}{\varepsilon_0\varepsilon_\infty m^* m_0}, \quad (2)$$

where N is the free carrier concentration, e is the elementary charge, ε_0 is the vacuum permittivity, m^* is the effective mass, and m_0 is the electron mass. In order to extract optical properties of the highly doped silicon, we consider plasma frequency and relaxation time as our fitting parameters.

A p-type commercial silicon wafer was used as a starting substrate to obtain black silicon texture. The randomly distributed needle-like nanostructures were obtained across the full wafer using a Bosch process consisting of cyclic steps. Each half cycle consists of (i) 10 s $SF_6 + O_2$ gas mixture based reactive ion etching (RIE), and (ii) 7 s C_4F_8 based deposition (passivation step), respectively. The etching process was carried out using an STS Multiplex ICP Etch system. Gas flow rates for SF_6, C_4F_8, and O_2 were 80 sccm, 70 sccm, and 5 sccm, respectively. The platen temperature was kept constant at 20 °C to fix the Si substrate temperature during the etching and deposition processes. The chamber pressure during etch step was kept constant at 35 mTorr. Similarly, the chamber pressure was kept constant at 20 mTorr during the deposition step. During the etch step, the coil power was set to 500 Watts, and platen power was set to 13 Watts. During the deposition step, the coil power was set to 400 Watts, and platen power was set to 0 Watts. Figure 1(a) shows two SEM images of one of the samples that is fabricated with 42 cycles of Bosch process. The top SEM image in figure 1(a) shows a sample whose middle section was intentionally removed out with focused ion beam milling in order to easily analyze the etching depth and texture of fabricated black silicon.

Due to random nature of black silicon texture, numerical simulations were conducted with approximate models of black silicon. In this work, structures on the black silicon sample were very similar to pyramidal structures as shown in the SEM images in figure 1(a). Therefore, we modeled black silicon structures as random pyramidal structures in simulation environment (figure 1(b)). We used an image processing software in order to determine the size distribution of the black silicon needles. EM wave simulations were performed using the finite difference time domain (FDTD) method. Three-dimensional simulation setup is constructed; on the x-axis and y-axis, periodic boundary conditions are used. On the z-axis (wave propagation direction) perfectly matched layer boundary condition is used. In all of the simulations, we employ cubic mesh with a mesh size of 10 nm.

Fabricated black silicon structures have pyramidal shapes with couple of micrometers in height, and couple of hundred nanometers (100–300 nm) in width. The widths of the structures are much smaller than the target wavelength range (5–10 μm). When EM wave interacts with structures much finer than its wavelength, rather than diffracting, it just reflects and transmits as if it is encountering a uniform medium [31]. Interaction of EM wave with such subwavelength structures can be described accurately by the EMT. We used Maxwell–Garnett effective medium approximation in this study [32]:

$$\varepsilon = \varepsilon_0\frac{f_m\sigma(\varepsilon_m - \varepsilon_0) + \varepsilon_m + \sigma\varepsilon_0}{\varepsilon_m + \sigma\varepsilon_0 - f_m(\varepsilon_m - \varepsilon_0)}, \quad (3)$$

where, ε is the effective permittivity of the medium, ε_0 is the permittivity of free space, σ is the screening parameter, ε_m is the permittivity of the material, and f_m is the fill ratio. In effective permittivity calculations, we used Drude model results for ε_m. Screening factor depends on the geometry of the structure and it can be approximated as unity for the structures with high aspect ratio as in our case. As shown in the fabricated samples, fill ratio of the black silicon texture gradually increases from top to the bottom. Therefore, in order to describe the structure we used multi-level profile as shown in figure 1(c). Each level has different fill ratio, and thus different effective permittivity. Consequently, we can model black silicon texture as a combination of uniform film stacks, each having finite film thickness. Finally the reflection and absorption of this multi-film structure can be calculated analytically by transfer matrix formalism (TMF).

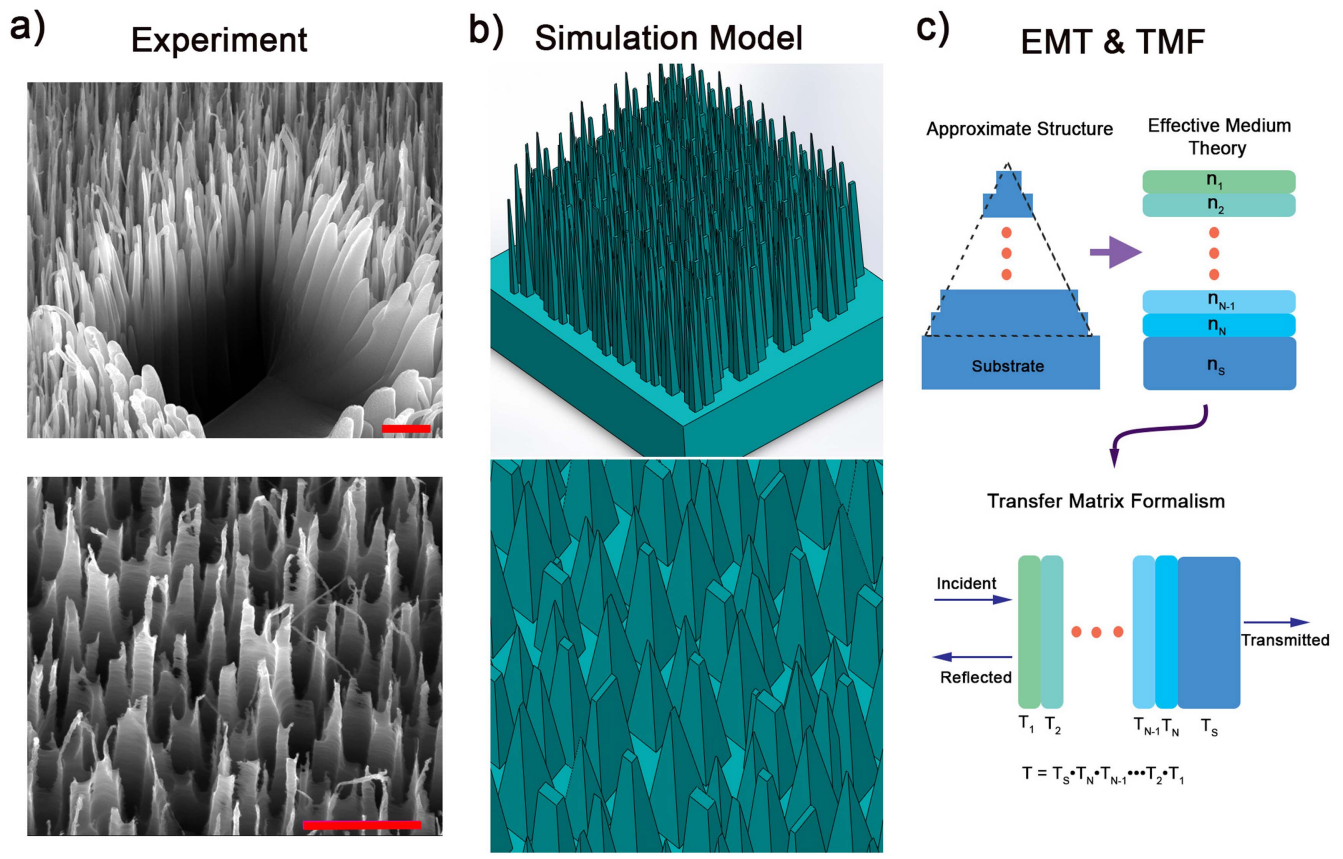

Figure 1. (a) SEM images of one of the fabricated samples. Scale bars are 1 μm (b) implementation of black silicon structure into the simulation environment. (c) Structural approximation of black silicon, effective medium theory (EMT) for this structure, and transfer matrix formalism (TMF).

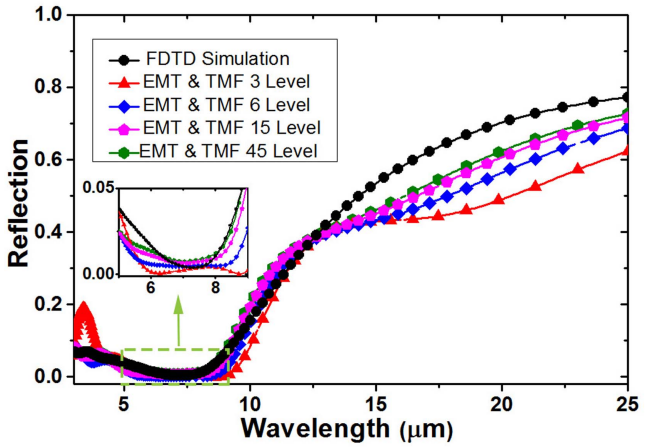

Figure 2. Simulated and analytically calculated reflection spectra of highly doped silicon with 7.5×10^{19} doping concentration, fill ratio 0–0.6. Analytical calculations conducted for different approximation levels.

3. Results and discussions

We first compare the simulated and the analytical reflection results. We extract the optical constants of a flat silicon wafer for simulations and analytical calculations. For the characterization of the optical properties of the silicon wafer J A Woollam IR-Vase Spectroscopic Ellipsometer is used. Ellipsometric data is modeled with Drude formalism to extract optical constants. We used periodic pyramidal structures with height of 3.5 μm on average. Periodicity of the unit cell is taken as 1500 nm and fill ratio of the structure is varied from 0 (at the tip of the pyramids) to 0.6 (at the bottom of the pyramids). Using the optical properties obtained from ellipsometric measurements, FDTD simulations were conducted. In order to conduct analytical calculations we first represent our structure as an effective film stack. Here the structure is approximated as N-level profile as illustrated in figure 1(c). The structure with height of 3.5 μm is divided into N layers where each layer has the same thickness $(3.5/N)$ but different fill ratio. Using the extracted optical constants of silicon we calculated the effective complex permittivity of the layers considering their fill ratio as a parameter in the Maxwell–Garnett effective medium approximation. Finally, the reflection and the transmission are calculated by TMF using the calculated complex permittivity values. Figure 2 shows simulated reflection and analytical calculations with 3-level, 6-level, 15-level, and 45-level approximations to the structure. As the number of divisions (levels) increases the profile of the theoretical model better resembles the simulated structure, thus the calculated reflection spectrum approaches to the simulated reflection spectrum. The Maxwell–Garnett effective medium approximation is valid for systems with low volume fractions [33]. In our case, fill ratio of the structure

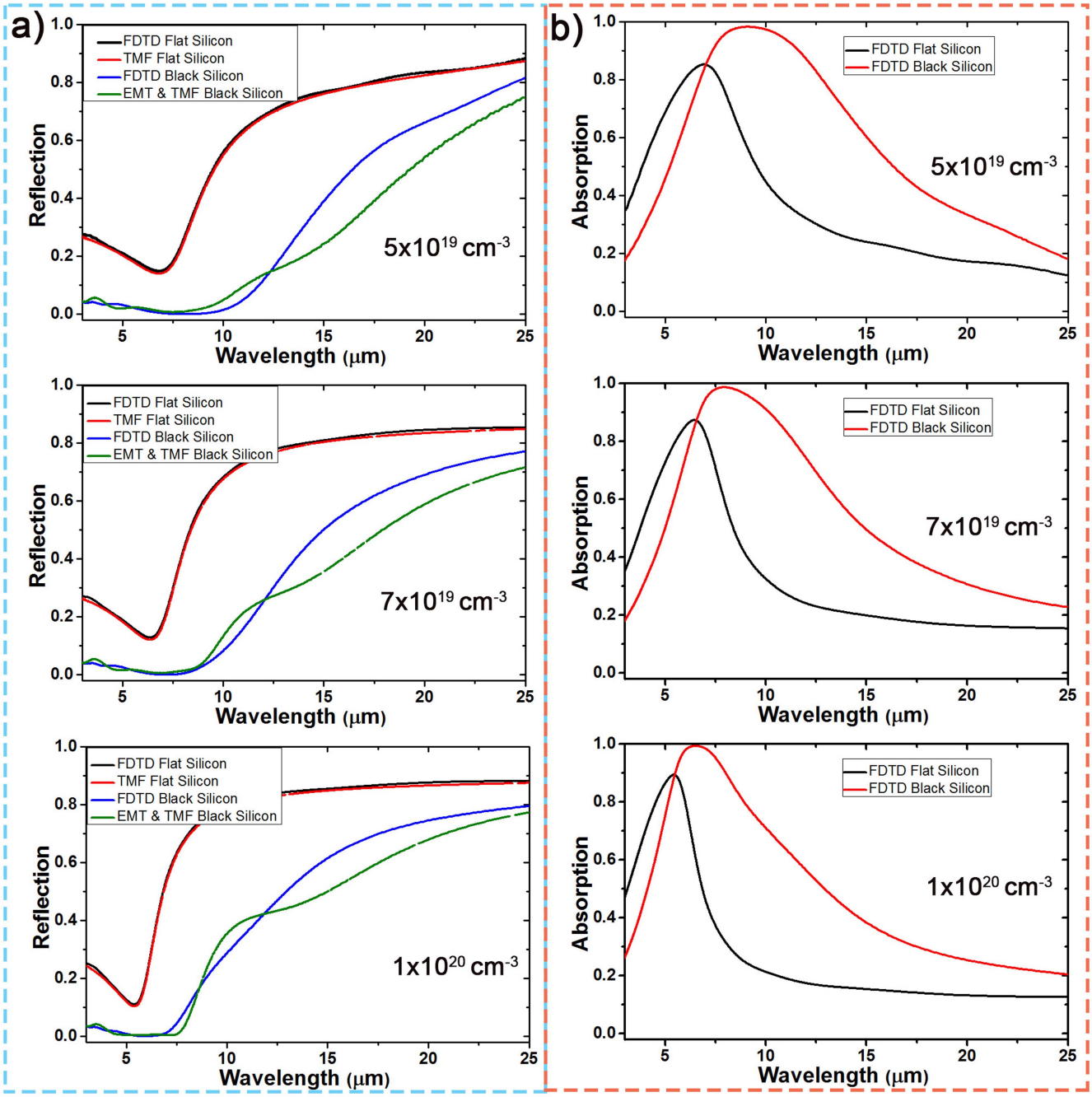

Figure 3. (a) Simulated and analytical reflection spectra of flat and black silicon for three different doping concentrations. (b) Simulated absorption spectra of flat silicon and black silicon with thickness of 4 μm for three different doping concentrations.

increases from top to bottom, thus the accuracy of the Maxwell–Garnett approximation is low at the bottom of the structure. The small difference between the analytical model and computational results is attributed to the Maxwell–Garnett effective medium approximation errors caused by relatively high volume fractions of the structure at the bottom.

Semiconductors are engineered materials and their optical properties can be tuned by controlling their carrier concentrations. Recently, active or passive tunable engineered semiconductor devices have been studied. Active tuning can be achieved by potential gating, while passive tuning can be achieved by doping [34–36]. Optical properties of highly doped silicon are dominated by different factors at low and high frequency limits. At low frequencies, as $\omega \backsimeq 0$, $1/\omega$ term dominates in the Drude model and imaginary part of the permittivity increases. Therefore, in low frequency regime, material behaves like a conductor. At high frequencies, $1/\omega^2$ term dominates in the Drude model and imaginary part of the permittivity decreases. Therefore in the high frequency regime, highly doped silicon behaves like low loss dielectric. Between low and high frequency regimes there is a characteristic transition frequency called plasma frequency at which material's optical response changes from dielectric to metallic. At the plasma frequency, the real part of the

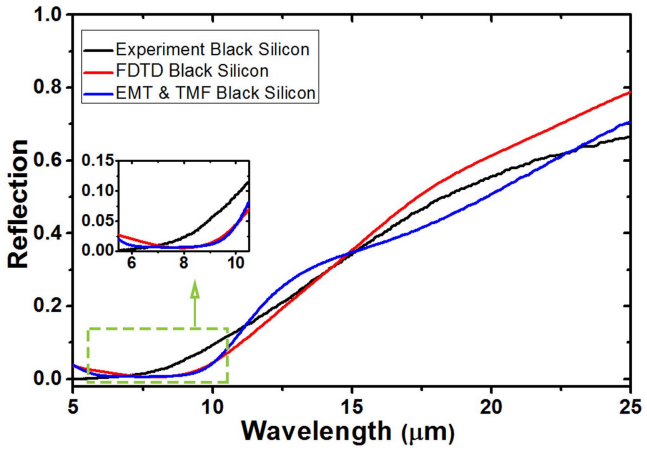

Figure 4. Experimental, simulated and analytical reflection spectra for the fabricated sample.

permittivity vanishes, but the imaginary part of the permittivity is still finite. Figure 3(a) shows the reflection spectra of black silicon and flat (non-structured) silicon structures for different doping concentrations. Clearly, the reflection from silicon surface is significantly reduced in the case of black silicon compared to the bare silicon. As expressed in equation (2) plasma frequency increases with increasing carrier concentration. Therefore, reflection minimum shifts to shorter wavelengths for both black and flat silicon structures with increasing carrier concentration. Around the plasma frequency, since the real part of the permittivity is very low, light can easily penetrate through the material and it is absorbed due to the finite absorption coefficient. Due to high loss coefficient of highly doped silicon, absorption occurs at the region very close to the surface. Figure 3(b) shows simulated absorption spectra of black and flat silicon structures for different doping concentrations. For practical applications, it is desirable to reduce the electrical thickness of the absorbers as much as possible without compromising its efficiency and bandwidth. Therefore, in these simulations absorption is calculated for 4 μm thick silicon, which is the optimal thickness providing wideband and near perfect absorption. As shown in the figure absorption peak of flat silicon makes a blue shift as doping concentration increases. Similarly, absorption peak of black silicon also makes a blue shift with increasing doping concentration, but in this case absorption efficiency and waveband considerably increased compared to that of flat silicon.

Reflection measurements of fabricated sample was taken with Bruker HYPERION 2000 IR microscope and Bruker Vertex 70v Fourier transform infrared spectrometer. The measurements are referenced to a gold-coated flat silicon mirror. Measured reflection spectrum of black silicon sample is shown in figure 4. Using optical constants FDTD simulations and analytical calculations were conducted. Simulated and analytical reflection spectra are also shown in figure 4. As shown in the figure, both simulated and analytical reflection spectra have similar trend with measured reflection spectrum.

4. Conclusions

In summary, we have demonstrated black silicon absorbers for mid-infrared applications. We fabricated our sample with a Bosch process which is allowing for cost-effective and wafer-scale fabrication. We showed that absorption spectrum can be tuned by controlling the doping concentration of silicon substrates. Fabricated black silicon structures were modeled both numerically and analytically. Both simulation results and analytical results well estimated the experiments. Silicon-based strong absorption of EM wave at mid-infrared region is very promising for realization of opto-electronic devices such as infrared imagers and sensors. Combined with extensive processing and device design knowledge base of silicon, presented absorbers yield fabrication simplicity and provide chip-scale integration compatible with CMOS technology.

Acknowledgments

This work was partially supported by the Scientific and Technological Research Council of Turkey (TUBITAK) under Grant No. 112E052. AKO acknowledges support from the Turkish Academy of Sciences Distinguished Young Scientist Award (TUBA GEBIP), BAGEP Award and FABED Award. KG acknowledges TUBITAK-BIDEB for MS scholarship.

References

[1] Aydin K, Ferry V E, Briggs R M and Atwater H A 2011 *Nat. Commun.* **2** 517
[2] Dereshgi S A and Okyay A K 2016 *Opt. Express* **24** 17644–53
[3] Watts C M, Liu X and Padilla W J 2012 *Adv. Mater.* **24** OP98–P120
[4] Nazirzadeh M A, Atar F B, Turgut B B and Okyay A K 2014 *Sci. Rep.* **4** 7103
[5] Atar F B, Battal E, Aygun L E, Daglar B, Bayindir M and Okyay A K 2013 *Opt. Express* **21** 7196–201
[6] Ding F, Cui Y, Ge X, Jin Y and He S 2012 *Appl. Phys. Lett.* **100** 103506
[7] Tao H, Bingham C M, Pilon D, Fan K, Strikwerda A C, Shrekenhamer D, Padilla W J, Zhang X and Averitt R D 2010 *J. Phys. D: Appl. Phys.* **43** 225102
[8] Avitzour Y, Urzhumov Y A and Shvets G 2009 *Phys. Rev.* B **79** 045131
[9] Ayas S, Güner H, Türker B, Ekiz O O, Dirisaglik F, Okyay A K and Dana A 2012 *ACS Nano* **6** 6852–61
[10] Zhong Y, Malagari S D, Hamilton T and Wasserman D 2015 *J. Nanophotonics* **9** 093791
[11] Naik G V, Shalaev V M and Boltasseva A 2013 *Adv. Mater.* **25** 3264–94
[12] Kesim Y E, Battal E and Okyay A K 2014 *AIP Adv.* **4** 077106
[13] Law S, Roberts C, Kilpatrick T, Yu L, Ribaudo T, Shaner E A, Podolskiy V and Wasserman D 2014 *Phys. Rev. Lett.* **112** 017401
[14] Shi C, Zang X, Wang Y, Chen L, Cai B and Zhu Y 2014 *Appl. Phys. Lett.* **105** 031104
[15] Chou L W, Shin N, Sivaram S V and Filler M A 2012 *J. Am. Chem. Soc.* **134** 16155–8

[16] Yin S, Zhu J, Xu W, Jiang W, Yuan J, Yin G, Xie L, Ying Y and Ma Y 2015 *Appl. Phys. Lett.* **107** 073903
[17] Kesim Y E, Battal E, Tanrikulu M Y and Okyay A K 2014 *Infrared Phys. Technol.* **67** 245–9
[18] Battal E, Bolat S, Tanrikulu M Y, Okyay A K and Akin T 2014 *Phys. Status Solidi* a **211** 2475–82
[19] Gorgulu K, Gok A, Yilmaz M, Topalli K and Okyay A K 2017 *J. Opt.* **19** 025002
[20] Gorgulu K, Gok A, Yilmaz M, Topalli K, Bıyıklı N and Okyay A K 2016 *Sci. Rep.* **6** 38589
[21] Gok A, Yilmaz M, Bıyıklı N, Topalli K and Okyay A K 2016 *J. Opt.* **18** 035002
[22] Steglich M, Lehr D, Ratzsch S, Käsebier T, Schrempel F, Kley E B and Tünnermann A 2014 *Laser Photonics Rev.* **8** L13–7
[23] Steglich M, Käsebier T, Zilk M, Pertsch T, Kley E B and Tünnermann A 2014 *J. Appl. Phys.* **116** 173503
[24] Liu X, Coxon P R, Peters M, Hoex B, Cole J M and Fray D J 2014 *Energy Environ. Sci.* **7** 3223–63
[25] Otto M *et al* 2015 *Adv. Opt. Mater.* **3** 147–64
[26] Deng Y L and Juang Y J 2014 *Biosens. Bioelectron.* **53** 37–42
[27] Gervinskas G, Seniutinas G, Hartley J S, Kandasamy S, Stoddart P R, Fahim N F and Juodkazis S 2013 *Ann. Phys., Lpz.* **525** 907–14
[28] Tikhonravov A V, Trubetskov M K, Amotchkina T V and Dobrowolski J A 2008 *Appl. Opt.* **47** C124–30
[29] Tikhonravov A V, Zhupanov V G, Fedoseev V N and Trubetskov M K 2014 *Opt. Express* **22** 32174–9
[30] Willey R R 2002 *Practical Design and Production of Optical Thin Films* (Charlevoix: CRC Press) (https://doi.org/10.1201/9780203910467)
[31] Raguin D H and Morris G M 1993 *Appl. Opt.* **32** 1154–67
[32] Foss C A Jr, Tierney M J and Martin C R 1992 *J. Phys. Chem.* **96** 9001–7
[33] Wang H, Liu X, Wang L and Zhang Z 2013 *Inter. J. Therm. Sci.* **65** 62–9
[34] Dionne J A, Sweatlock L A, Sheldon M T, Alivisatos A P and Atwater H A 2010 *IEEE J. Sel. Top. Quantum Electron.* **16** 295–306
[35] Li D and Ning C Z 2011 *Opt. Express* **19** 14594–603
[36] Liu X L, Wang L P and Zhang Z M 2013 *J. Heat Transfer* **135** 061602